Journal of Molecular Liquids 332 (2021) 115868

Contents lists available at ScienceDirect

Journal of Molecular Liquids

journal homepage: www.elsevier.com/locate/molliq

Effects of insecticide acephate on membrane mimetic systems: The role played by electrostatic interactions with lipid polar headgroups

Luis F.C. Morato [a], Gilia C.M. Ruiz [a,*], Wallance M. Pazin [a], Orisson P. Gomes [b], Osvaldo N. Oliveira Jr [c], Augusto Batagin-Neto [d], Carlos J.L. Constantino [a]

[a] Department of Physics, School of Technology and Applied Sciences, São Paulo State University (UNESP), Presidente Prudente, SP, Brazil
[b] São Paulo State University (UNESP), School of Sciences, POSMAT, 17033-360 Bauru, SP, Brazil
[c] São Carlos Institute of Physics, University of São Paulo (USP), São Carlos, SP, Brazil
[d] São Paulo State University (UNESP), Campus of Itapeva, 18409-010 Itapeva, SP, Brazil

ARTICLE INFO

Article history:
Received 8 September 2020
Received in revised form 14 January 2021
Accepted 5 March 2021
Available online 08 March 2021

Keywords:
Langmuir monolayers
Lipid vesicles
Membrane model
PM-IRRAS
Acephate
Molecular modeling

ABSTRACT

Pesticides are important agrochemicals to yield high crop productivity but their indiscriminate use may harm the environment and human health. In order to seek a compromise between effectiveness as insecticide and safety for humans, it is essential to correlate their physiological action with molecular-level interaction with cell membranes. In this study, we found that acephate interacts preferentially with positively charged Langmuir monolayers that represent simplified cell membranes. This was proven by comparing surface pressure-molecular area (π-A) isotherms and polarization-modulated infrared reflection absorption spectroscopy (PM-IRRAS) data on monolayers of the zwitterionic 1,2-dipalmitoyl-sn-glycerol-3-phosphocholine (DPPC) and 1-palmitoyl-2-oleoyl-glycero-3-phosphocholine (POPC), the cationic dimethyldioctadecyl ammonium bromide (DODAB) and 1,2-dipalmitoyl-3-trimethylammonium-propane (DPTAP), and the anionic dihexadecyl phosphate (DHP) and 1,2-dipalmitoyl-sn-glycero-3-phosphate (DPPA). While acephate induced a closer packing of DODAB and DPTAP monolayers upon binding to their quaternary ammonium and choline groups, respectively, almost no effects were observed in the π-A isotherms of the other lipids. Such preferred interaction between acephate and the positively-charged groups was confirmed with density-functional theory (DFT) calculations. Acephate also changed the size and zeta potential of large unilamellar vesicles (LUVs) formed with cationic lipids. Taken together these results point to a physiological action related to acephate binding to positively charged groups owing to its negative character, which may help establish conditions for the safe use of this insecticide.

1. Introduction

The organophosphate insecticide acephate is used in food crops, agricultural seeds and non-flowering plants, and it acts on the tissues of the nervous system of sucking and biting insects, leading them to death [1]. Due to its toxicity to humans [2,3], acephate was banned in Europe but it is available in the United States and in some developing countries [4,5]. In Brazil, for instance, its use is restricted to specific plantations and to low concentrations, but these restrictions are often ignored. In fact, there is evidence that in 2017 and 2018 acephate was the pesticide with the highest degree of irregular use in the country [5], which is worrying because Brazil is the second largest exporter of agricultural products in the world [6]. Even though acephate has been used on a large scale and indiscriminately, its potential damage to humans has been investigated only in a few in vivo studies [7–9] and autopsies [10]. Acephate inhibits acetylcholinesterase in the hydrolysis of the neurotransmitter acetylcholine, which is linked to several neural disorders [11–13], and its damaging effects involve metabolic pathways [10]. The inhibition is believed to arise from an electrostatic interaction between the negatively charged acephate groups and positively charged groups of acetylcholinesterase [12]. It is therefore essential to study the interaction mechanisms of acephate with cell structures at the molecular level, especially the plasma membrane that defines the cell boundaries and internal organelles [14]. Studies correlating in vivo and in vitro effects of acephate in mice cells revealed the difficulty to achieve a detailed understanding of such interactions [1]. These limitations are due to the complexity of the cell structure, which can be circumvented using simple models of self-organized lipids (mono or bilayers) that mimic the plasma membrane [15–17].

In this paper, we investigate the effects of acephate on Langmuir films (lipid monolayers), large and giant unilamellar vesicles (LUVs and GUVs). The first mimics one leaflet of the plasma membrane, while LUVs and GUVs represent lipid self-assembled bilayers as in membranes, with the size of GUVs being comparable to eukaryotic cells [18]. A judicious choice was made of the lipids to form the

* Corresponding author.
E-mail address: gilia.ruiz@unesp.br (G.C.M. Ruiz).

https://doi.org/10.1016/j.molliq.2021.115868
0167-7322/

monolayers and bilayers in order to verify whether acephate has preferential interaction with charged groups. The lipids chosen (see Fig. 1) were the zwitterionic 1,2-dipalmitoyl-sn-glycerol-3-phosphocholine (DPPC) and 1-palmitoyl-2-oleoyl-glycero-3-phosphocholine (POPC), dimethyldioctadecyl ammonium bromide (DODAB), dihexadecyl phosphate (DHP), 1,2-dipalmitoyl-3-trimethylammonium-propane (DPTAP) and 1,2-dipalmitoyl-sn-glycero-3-phosphate (DPPA). DPPC and POPC were selected because phosphatidyl cholines represent ~50% in mass in eukaryotic cells (organelles and plasma membranes) [19–24]. DODAB and DPTAP have positively charged groups while DPPA and DHP are anionic, then allowing us to test the hypothesis of direct action from acephate in charged structures. In order to have a more comprehensive body of data for the analysis we combine surface pressure-molecular area (π-A) isotherms, Brewster Angle Microscopy (BAM) and polarization-modulated infrared reflection absorption spectroscopy (PM-IRRAS) measurements in Langmuir monolayers, zeta potential and dynamic light scattering (DLS) in LUVs and phase contrast microscopy in GUVs.

2. Materials and methods

2.1. Materials

DPPC, DHP, DPTAP, DPPA, and POPC were purchased from Avanti Polar Lipids, and DODAB was purchased from Fluka. All materials were of analytical grade (> 99%). Acephate, chloroform, methanol, and polyvinyl alcohol (PVA - MW: 146,000–186,000) were purchased from Sigma-Aldrich. Aqueous solutions and subphases were prepared using ultrapure water (Mili-Q system, resistivity 18.2 MΩ.cm^{-1}).

2.2. π-A isotherms

A KSV Langmuir trough, model 2000 (40 mL subphase, 150 cm^2) was used to obtain the π-A isotherms of the lipid films. The lipids were dissolved in a mixture of chloroform and methanol (7:3, v:v) at a concentration of 0.5 mg.mL^{-1}. An aliquot of this solution was spread onto the subphase containing either ultrapure water or an aqueous solution of acephate (10^{-4} M). In subsidiary experiments we employed a higher concentration of 10^{-3} M (below its solubility in water at 25 °C: 4.46×10^{-3} M) of acephate but the effects did not change to any significant extent, which is why all the results to be presented in this paper were obtained only with 10^{-4} M. After organic solvent evaporation (15 min), the barriers compressed the monolayer at 10 mm.min^{-1}, and the π-A isotherms were measured. The in-plane elasticity of the monolayers was calculated from the isotherms using the compressional modulus ($Cs^{-1} = -A\left(\frac{\partial \pi}{\partial A}\right)_T$, where A is the mean molecular area and π is the surface pressure.

2.3. Brewster angle microscopy (BAM)

BAM measurements were carried by using an Accurion Nanofilm EP4 Brewster-angle microscope (Goettingen, Germany) coupled to a Langmuir trough (KSV Instruments Ltd., Helsinki, Finland). The monolayers of DODAB, DPTAP or DPPC were formed under the same

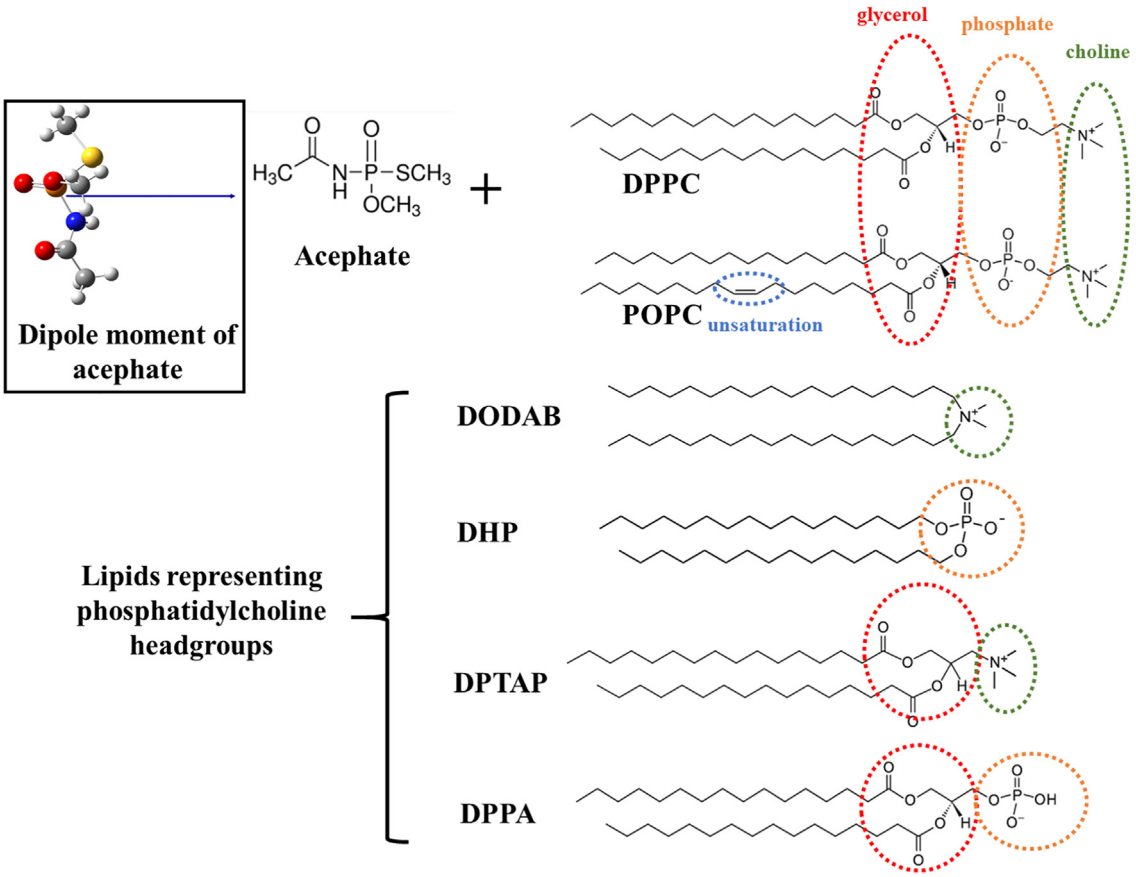

Fig. 1. Molecular structures of acephate and lipids: 1,2-dipalmitoyl-sn-glycerol-3-phosphocholine (DPPC); 1-palmitoyl-2-oleoyl-glycero-3-phosphocholine (POPC), dimethyldioctadecylammonium bromide (DODAB); dihexadecyl phosphate (DHP); 1,2-dipalmitoyl-3-trimethylammonium-propane (DPTAP) and 1,2-dipalmitoyl-sn-glycero-3-phosphate (DPPA). Up-left corner: dipole moment vector of acephate obtained by (DFT) calculations (|μ| = 7.05 D). The atoms are represented by spheres: yellow – sulfur; orange – phosphorus; red – oxygen; blue – nitrogen; gray – carbon; and white – hydrogen.

conditions as for the π-A isotherms. A polarized 658 nm laser, focusing on the air-water interface with an incident angle of 53.1° (Brewster angle), and a charged-coupled-device (CCD) camera were used to capture the images at different surface pressures.

2.4. PM-IRRAS measurements

The PM-IRRAS experiments were performed with a KSV PMI 550 instrument (Finland) coupled to a Langmuir trough. The DODAB, DPTAP and DPPC Langmuir films (at $\pi = 30$ mN.m^{-1}) were obtained in the absence and presence of acephate in the aqueous subphase. The spectra were acquired by focusing an infrared beam (80° relative to the normal) polarized in two plans (*p*: parallel to the incidence plan; *s*: perpendicular to the incidence plane) at subphase surface. The signal (S) is calculated as (Rp-Rs)/(Rp + Rs), where Rp and Rs are the reflectance of polarizations *p* and *s*, respectively. PM-IRRAS background signals were acquired for ultrapure water (in the absence of acephate) and 10^{-4} M acephate solution subphase.

2.5. Preparation of large and giant unilamellar vesicles

To facilitate swelling of GUVs formed of cationic lipids, we adopted the methodology described by Martins et al. [25]. Briefly, a solution of DODAB or DPTAP (10 mM) in methanol:chloroform (1:3 – v:v) was dried in a test-tube under N_2 gas with a vortex. The films were left under vacuum for 1 h to remove solvent traces. A sucrose solution (0.2 M) previously heated to 80 °C was added to the dried films. The hydrated films were left under heating (80 °C) during 20 min and vortexing every 5 min. GUVs of DPPC were obtained as proposed by Angelova et al. [26,27]. An aliquot of 8 μL of DPPC solution (1 mM) was spread in two parallel platinum wires coupled in a Teflon chamber. The system was dried in vacuum for 1 h to evaporate the solvent of the lipid solution and then hydrated with a heated sucrose solution (0.2 M) at 60 °C (above the phase transition temperature of DPPC [28]). The Teflon chamber was biased with 1 V at 10 Hz for at least 1 h to yield the electroformation of GUVs. The POPC vesicles were prepared using the method by Weinberger et al. [29]. The experimental procedure consists of spreading 400 μL of PVA aqueous solution (5% *w*/w) in a beaker and let it dry at a temperature higher than 50 °C in the oven. Then, 10 μL of 1 mM POPC chloroform solution were added in the beaker with dried PVA and taken again to dry in a vacuum chamber for 1 h. For the GUVs to swell, 500 μL of sucrose solution were added for 90 min.

Aliquots of 50 μL of the suspension containing GUVs of DODAB, DPTAP, DPPC and POPC were added to an eight-well polymer chamber containing 200 μL glucose solution (0.2 M) or glucose mixed with acephate solution ($0.2\ M/1 \times 10^{-4}$ M – acephate final concentration in the chamber with GUVs is 0.8×10^{-4} M). The osmolarity of sucrose and glucose solutions was measured using an osmometer (Osmomat 3000, Gonotec, Germany), and the concentration should be the same on the inner and outer portions of GUVs. Thus, possible changes in the vesicle morphology cannot be associated to differences in osmolarity. The phase contrast images were obtained with a Nikon C2/C2si Eclipse Ti-E (Kyoto, Japan) optical microscope, using a 40× air objective. Videos lasting 30 min were acquired in triplicate and 5 photos were taken for each measurement to count the number of GUVs affected by the pesticide.

Large unilamellar vesicles (LUVs) formed with DODAB, DPTAP and DPPC were prepared from stock solutions of chloroform at 2 mM. Dry films of each lipid were obtained by evaporating the solvent under a N_2 flow, and the remaining traces of the organic solvent were eliminated by placing the dried films under reduced pressure for at least 1 h. Lipids were resuspended in pre-heated ultrapure water (at a temperature above the thermal phase transition) to a concentration of 2 mM to form multilamellar vesicles (MLVs). LUVs were obtained with subsequent extrusion passing the MLVs suspensions through 0.4 and 0.1 μm polycarbonate membranes (Whatman, Sigma Aldrich) for 8 and 15 times, respectively. Finally, aliquots of LUVs suspension for each lipid were added in ultrapure water or acephate solution (0.1, 10, 25, 50, 75 or 100 μM) to reach the final concentration of 100 μM. These systems were characterized by Dynamic Light Scattering (DLS) and Zeta Potential (Zetasizer Nano ZS90) at 25 °C to evaluate the size and surface charge of the vesicles, respectively.

2.6. Molecular modeling

Electronic structure calculations were conducted for all compounds (acephate and lipids) to evaluate local reactivities, electrostatic potentials and adsorption (binding) energies. The calculations were conducted in the framework of density functional theory (DFT) using B3LYP [30–33] and CAM-B3LYP [34] exchange-correlation functionals (for isolated and adsorbed systems, respectively) and 6-31G(d,p) basis set. The presence of the solvent (water) was simulated via polarizable continuum method (PCM) [35]. Gaussian 16 [36] computational package was employed for geometry optimizations/calculation of properties and Orca 4.0 [37] for the calculation of adsorption energies. DFT-based approaches on simplified acephate+lipid models were preferred to classical methods to assess molecular features of the pesticide and lipids. Hence, lipid/lipid interactions are not explicitly described, being instead estimated from the electrostatic maps and local reactivities.

The local reactivities of the compounds were evaluated via condensed-to-atoms Fukui indexes (CAFI) [38,39] and molecular electrostatic potential (MEP) maps. CAFIs are defined in the framework of conceptual DFT and can be employed to evaluate molecular interactions involving the frontier molecular orbitals of the compounds (called as soft-soft interactions) and identify the most reactive sites of the molecules in relation to electrophilic (f^-) and nucleophilic (f^+) external agents [40]. On the other hand, MEP maps allow us to identify electron rich and electron deficient regions of the molecules which are relevant to predict electrostatic interactions (called hard-hard interactions). CAFIs were estimated via a finite difference approximation, considering the electronic populations of the atoms in neutral, anionic and cationic configuration of the molecules [41,42]. Hirshfeld's partition charge method was employed to estimate the electronic populations to avoid negative indices [43,44]. The MEP color maps were estimated from the atomic charges from CHelp scheme [45].

Adsorbed (acephate+lipid) systems were evaluated via DFT/CAM-B3LYP/6-31G(d,p) approach to estimate the binding energies and changes in CAFI and MEPs. The structures were initially designed by aligning negatively and positively charged sites of the acephate and lipids (DPPC, DODAB and DPTAP). Adsorption (or binding) energies were estimated considering the difference in the total energies of adsorbed (A + L) and isolated (A and L) compounds, before and after adsorption, eliminating the basis set superposition error (BSSE) with the counterpoise method [46], i.e.:

$$E_{ADS} = E^{A+L}_{A+L}(A+L) - \left[E^{A}_{A}(A) + E^{L}_{L}(L)\right] - \Delta E_{BSSE} \quad (1)$$

$$\Delta E_{BSSE} = \left(E^{A+L}_{A}(A+L) - E^{A+L}_{A}(A)\right) + \left(E^{A+L}_{L}(A+L) - E^{A+L}_{L}(L)\right) \quad (2)$$

where $E^{Y}_{X}(Z)$represents the total energy of fragment X, calculated at the optimized geometry of fragment Y and considering the basis set of fragment Z. In our case, A + L, A and L represent the acephate + lipid (adsorbed system), acephate and lipid, respectively. This approach eliminates the artificial (mathematical) stabilization of A + L systems due to the use of additional basis set of L to describe the electronic configuration of A (and vice versa).

3. Results and discussion

3.1. Acephate interactions with lipid Langmuir monolayers

Fig. 2 shows the π-A isotherms for DODAB, DPTAP and DPPC obtained on ultrapure water (solid lines) and in an acephate subphase

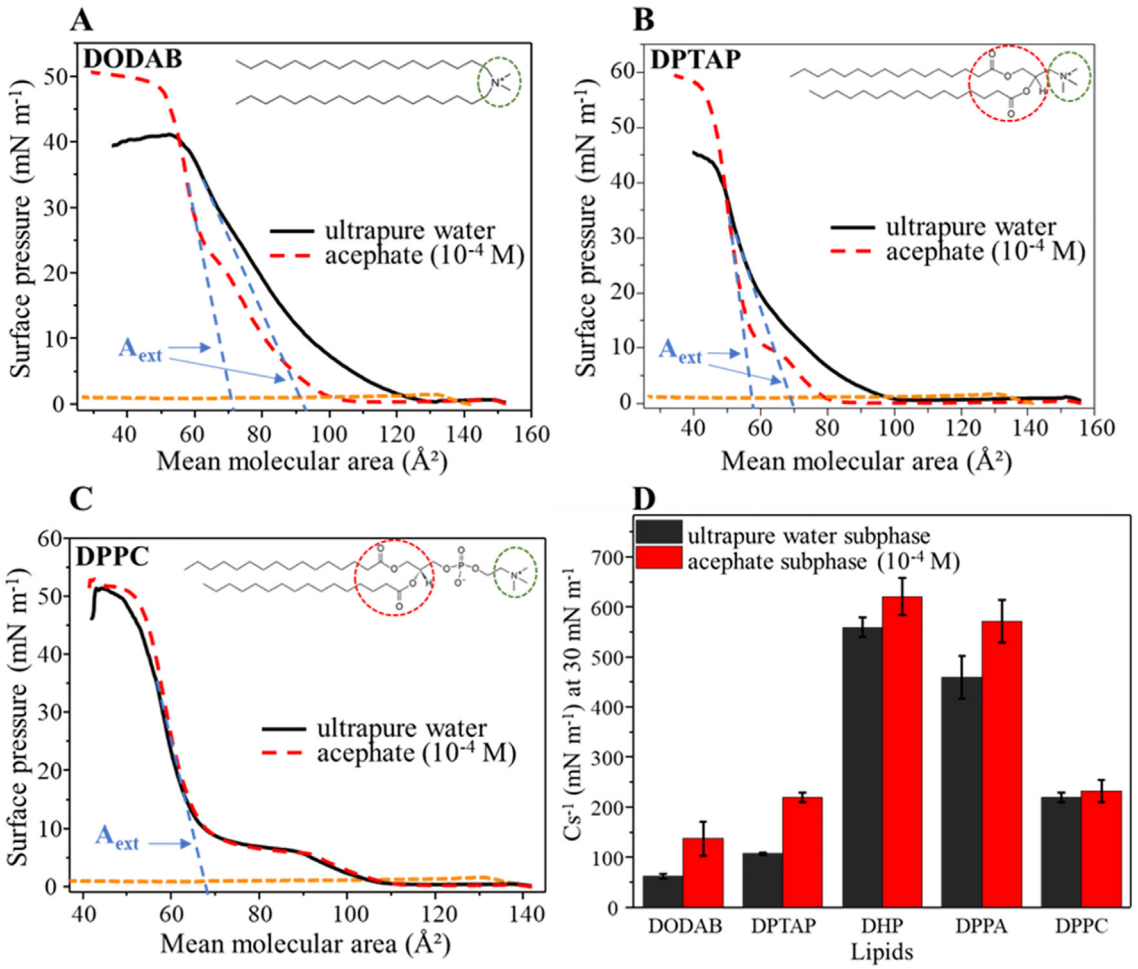

Fig. 2. π-A isotherms for the lipids **(A)** DODAB; **(B)** DPTAP; and **(C)** DPPC in the absence and presence of acephate (10^{-4} M) on subphase. The extrapolated area (A_{ext} - from the highest lipid packing to zero pressure) is represented by a blue dashed line. The orange dashed line indicates that acephate molecules do not form Langmuir films on their own. **(D)** Compressional modulus from π-A isotherms of the lipid films in the absence and presence of acephate.

(10^{-4} M - dashed lines). The π-A isotherms in ultrapure water are consistent with the literature [47]. To examine the effects from acephate, the extrapolated area (E_A) was determined by tracing a line from the region of highest lipid packing to zero pressure. The decrease in extrapolated area (ΔA_{ext}) induced by acephate was 25 Å^2 for DODAB and 23 Å^2 for DPTAP monolayers. The π-A isotherms of DPPC, and the anionic lipids DHP and DPPA are not shifted by acephate (Figs. S1 A and B, respectively). This reveals the preferential interaction between acephate and positively charged monolayers. Acephate might surround the quaternary ammonium group (N^+), decreasing electrostatic repulsion between DODAB polar headgroups and yielding a more closely-packed monolayer. The similar trend for DODAB and DPTAP indicates that acephate interacts with DPTAP choline ($CN^+(CH_3)_3$) group. The shift at 30 mN.m^{-1}, which corresponds to the lateral pressure of plasma membranes [48,49], is more prominent for DODAB than for DPTAP monolayer. This difference is probably due to the stronger repulsive interactions between DODAB molecules, which has only the positive group in its head. DPTAP also has a glycerol group that can increase the cohesive forces and diminish the DPTAP-DPTAP electrostatic repulsion. This repulsion is reflected by the larger mean molecular area for which the surface pressure starts to rise for the ultrapure water subphase (DODAB: 129 Å^2; DPTAP: 103 Å^2).

The lack of changes in the DPPC monolayer may indicate that acephate could be placed underneath the monolayer, surrounding the choline ($CN^+(CH_3)_3$) group, and/or be located at within the headgroup region without occupying an area at the air/water interface. The reason why a decrease in molecular area of DPPC is not induced by acephate might be related to the volume occupied by glycerol and phosphate groups and/or to the repulsion between DPPC phosphate groups. In DPPC the presence of phosphate promotes a more repulsive environment than DPTAP (the surface pressure starts to rise at 110 Å^2 for DPPC), but less repulsive than DODAB. Acephate does not promote any shift at 30 mN.m^{-1} for DPPC, whose area remains at 58 Å^2. Another important feature is the increase in monolayer stability [50] caused by acephate, as revealed by the increase in collapse pressure for DODAB (41 to 49 mN.m^{-1}) and DPTAP (45 to 59 mN.m^{-1}). This effect is not observed for DPPC, which is consistent with the previous discussion on the balance of attraction/repulsion interactions involving DPPC and acephate.

A shift to smaller areas in π-A isotherms has been observed with incorporation of gold nanoparticles in the subphase for DPPC, DODAB, dipalmitoylphosphatidylglycerol (DPPG), dioleoylglycerophosphocholine (DOPC), and cholesterol [51] and of KBr for DODAB [52]. Similarly to the interpretation of the acephate results, the shifts were attributed to a decreased repulsion between lipid headgroups caused by gold nanoparticles or Br^- ions.

The compressional modulus at 30 mN.m^{-1} in Fig. 2-D shows no effect from acephate on the DPPC monolayer which remains in the liquid-condensed (LC) phase [53]. The monolayer packing caused by acephate in DODAB and DPTAP resulted in a drastic change of Cs^{-1}:

from 63 ± 5 to 138 ± 34 mN.m^{-1} for DODAB (219%), which implies in a LE-LC (liquid-expanded to liquid-condensed) phase transition, and from 108 ± 2 to 220 ± 9 mN.m^{-1} for DPTAP (204%). A change in the π-A isotherm slope is noticed at 21 mN.m^{1} for DODAB and 9 mN.m^{-1} for DPTAP. As for the anionic lipids, although the π-A isotherms for DHP and DPPA monolayers have not been affected by acephate, changes were observed in Cs^{-1} from 560 ± 20 to 621 ± 37 mN.m^{-1} (111%) and from 460 ± 43 to 572 ± 42 mN.m^{-1} (124%), respectively. Therefore, the presence of acephate in the subphase increases monolayer rigidity for all lipids with residual charge. All Cs^{-1} graphics are present in Fig. S2.

A molecular-level study was performed by means of PM-IRRAS for the interaction of acephate with DODAB and DPTAP monolayers. Although π-A isotherms suggest acephate does not alter DPPC monolayers, an analysis was also performed to compare the effects with the positively charged lipids. Fig. 3 shows the PM-IRRAS spectra of DODAB monolayer at 30 mN.m^{-1} on ultrapure water (solid black line) and acephate solution (10^{-4} M - dashed red line). The main vibration band of DODAB polar headgroup is assigned to C—N stretching at 913 cm^{-1} [54], which is shifted to 925 cm^{-1} by acephate owing to ion-dipole interactions with the positively charged quaternary ammonium group (N^+). This should be expected from the affinity between acephate and DODAB positive group inferred from discussion of the π-A isotherms. In DPTAP, acephate induces a shift from 943 to 953 cm^{-1} in the band assigned to choline ($\upsilon_{as}(CN^+(CH_3)_3)$, as shown in Fig. 4-A, consistent with an ion-dipole attraction between the positive choline group and acephate. Besides, the shift of the glycerol (υC=O) band from 1730 to 1740 cm^{-1} suggests a weakening of the H-bonding network around this group [55,56], probably as a consequence of the presence of acephate molecules. The effect from acephate on the organization of the alkyl chains can be probed by calculating the relative band intensity between the symmetric and antisymmetric stretchings of CH_2 (RI = $\upsilon_s CH_2$ intensity/$\upsilon_{as} CH_2$ intensity): the lower the relative intensity, the higher the alkyl chain ordering [57]. RI is barely changed by acephate for DODAB (RI_{water} = 0.55 and $RI_{acephate}$ = 0.52) in Fig. 3-B, i.e. the orientation of DODAB aliphatic chains remains the same. In contrast, for DPTAP in Fig. 4-B a decrease is seen from RI_{water} = 0.64 to $RI_{acephate}$ = 0.48 as acephate induces an increased order of the hydrophobic chains.

The assignments of the main vibrational modes of polar headgroups of DPPC in Fig. 5-A are in accordance with the literature [51,58]. The band at 970 cm^{-1} attributed to the antisymmetric stretching of choline group ($\upsilon_{as}(CN+(CH_3)_3)$) [58] shifts to 963 cm^{-1} with acephate in the subphase. Therefore, despite the lack of changes in π-A isotherms, there might be an ion-dipole attractive interaction between the DPPC cationic headgroup (choline) and acephate. On the other hand, an ion-dipole attractive interaction could also be expected between the positive portion of acephate molecule and phosphate in the DPPC headgroup. This interaction may have caused the splitting of the 1076 cm^{-1} band assigned to C-O-PO_2 moiety into bands at 1055 and 1085 cm^{-1}. The δCH_2 and υC=O bands (at 1464 and 1737 cm^{-1}, respectively) of DPPC glycerol group were not affected significantly, suggesting that acephate might be surrounding the choline and phosphate headgroups, preferentially. The bands assigned to symmetric and antisymmetric stretching of CH_2 group (2850 and 2920 cm^{-1}) at the tails of DPPC are shown in Fig. 5-B. An increase in relative intensity from RI_{water} = 0.46 to $RI_{acephate}$ = 0.65 reveals an increase of the DPPC alkyl chain disorder induced by acephate.

3.2. Molecular modeling

The acephate-lipid interactions were evaluated in detail using DFT calculations for the local reactivity of isolated and adsorbed systems. Fig. 6 illustrates the colored maps for CAFI and MEP descriptors for acephate, DPPC, DODAB and DPTAP. Red regions define the most reactive and negatively (or less positively*) charged sites, for CAFI and MEP, respectively, while blue regions define nonreactive or (more*) positively charged sites. Similar maps are presented in the Supplementary Material for all the lipids. Owing to the absence of spatial restrictions imposed by adjacent structures, the lipid tails presented an "opened" conformation after geometry optimization via DFT-based calculations. A preliminary evaluation of DPPC with distinct relative positions of the tails shows that the reactivity descriptors in Fig. 6 are insensitive to such arrangement (see Fig. S3), so that similar results are expected for structures with vertically aligned tails.

Overall, the CAFI and MEP maps in Fig. 6 reinforce the preferential interaction between acephate and lipids with positive heads. Acephate possesses an intense electron-rich region centered on the oxygen

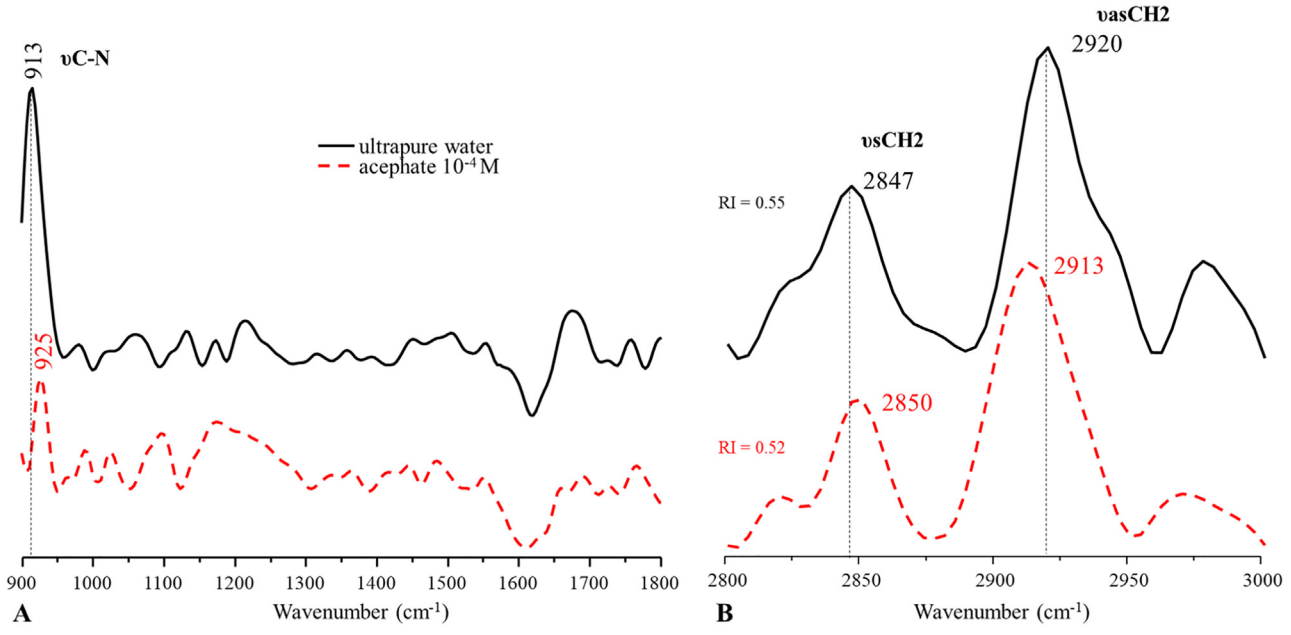

Fig. 3. DODAB PM-IRRAS spectra of **(A)** polar head region and **(B)** hydrocarbon chains region. The solid black lines represent the spectra in the subphase of ultrapure water and the red dashed ones are the spectra in the presence of acephate (10^{-4} M). RI: relative intensity.

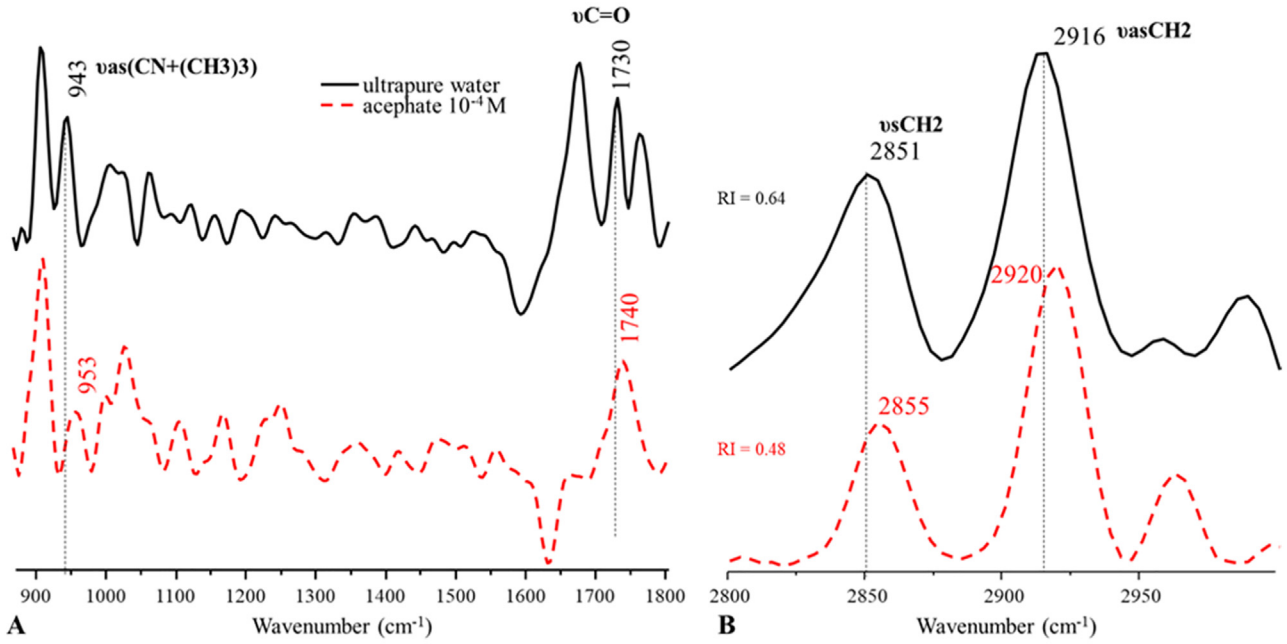

Fig. 4. DPTAP PM-IRRAS spectra of **(A)** polar head region and **(B)** hydrocarbon chain region. The solid black lines represent the spectra for ultrapure water and the red dashed ones refer to the spectra in the presence of acephate (10^{-4} M). RI: relative intensity.

atoms (attached to P), while the positive charges are spread out over the molecule, mainly on the hydrogen atoms of -NH and -CH_3. The spatial restriction of an intense negative potential at the oxygens can facilitate the interaction with positively charged structures. Moreover, since the positive potential is linked to terminal methyl groups, it should be more sensitive to thermally-induced structural changes, hindering the effective interactions of acephate with negatively charged structures.

Another relevant feature inferred from Fig. S4 is that acephate-lipid interactions are supposed to be governed by electrostatic effects (hard-hard interactions) as effective acephate-DPPA interactions (via $S(f^+)$- phosphate(f^-)) should be expected from the evaluation of CAFI indexes.

The reactivity and adsorption energies of acephate+lipid (adsorbed) systems were estimated using DFT, with structures designed by aligning

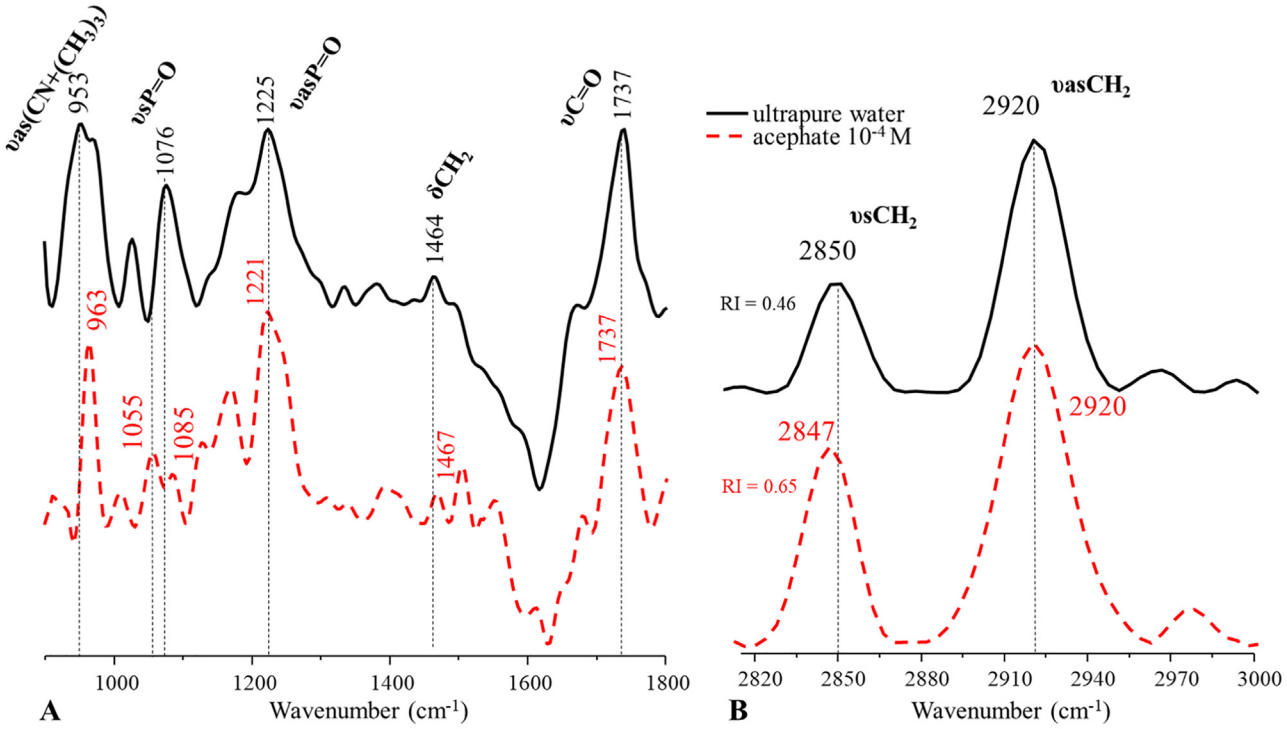

Fig. 5. DPPC PM-IRRAS spectra of (**A**) polar headgroup and (**B**) hydrocarbon chains region. The black lines represent the spectra for ultrapure water and the red dashed ones refer to the spectra in the presence of acephate (10^{-4} M). RI: relative intensity.

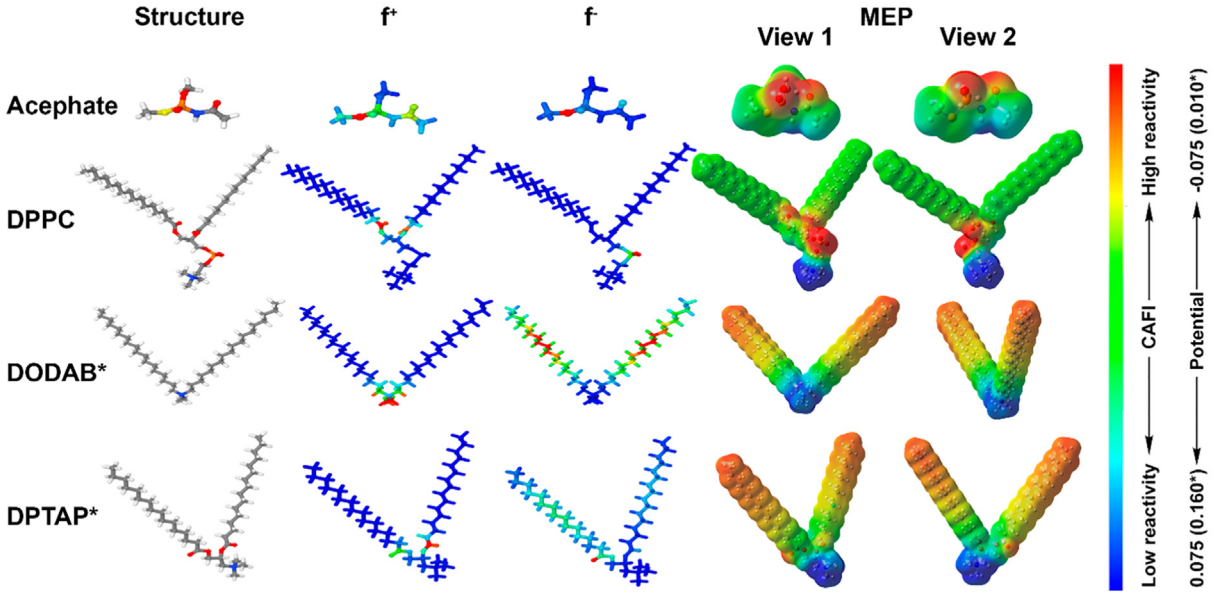

Fig. 6. Color maps for the local reactivity of acephate, DPPC, DODAB and DPTAP. f^+ and f^- define reactive sites towards nucleophiles and electrophiles, respectively. The structures containing MEPs were rotated to facilitate visualization.

negatively and positively charged sites of acephate and lipids (DPPC, DODAB and DPTAP). The results summarized in Fig. 7 (with the same color scale of Fig. 6) and Table 1 indicate that acephate induces a significant reduction in potential around the lipid heads, with very small effects on the tails. The adsorption process can lead to two competing effects: i) reduction of the repulsive forces between the lipid heads allowing their approximation; ii) additional spatial restriction to the approximation of these structures. These effects are more evident for DODAB and DPTAP. In DPPC acephate alters the charge balance of the zwitterionic region, which is relevant for the interaction of adjacent lipidic units. Given the effective interaction between oxygen atoms and choline groups of the lipids, after adsorption it is noticed that reactive sulfur atoms (towards electrophiles, i.e. with high f-) are exposed to the adjacent units in all cases, suggesting that soft-soft interactions could act as an additional cohesive process.

Table 1
Adsorption energies for each system in the gas phase and in water.

System	Adsorption energy (kcal/mol)	
	Gas phase	In water
Acephate + DPPC	−47.508	−19.545
Acephate + DODAB	−21.535	−6.682
Acephate + DPTAP	−24.567	−8.281

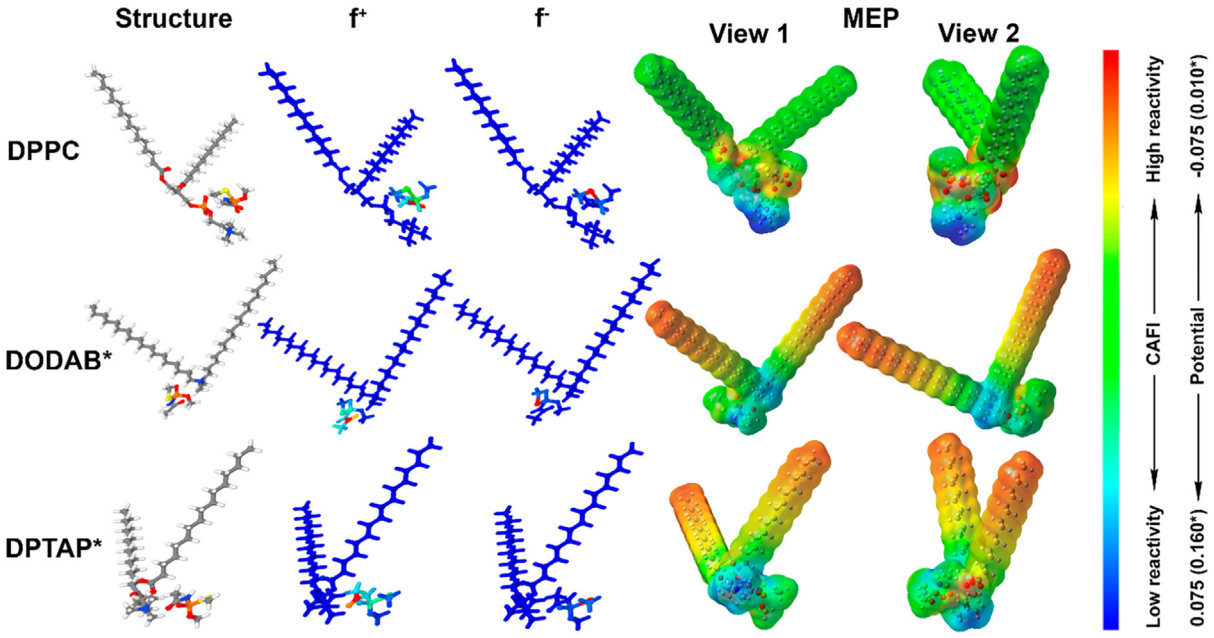

Fig. 7. Color maps for local reactivity of adsorbed systems: acephate+DPPC, acephate+DODAB and acephate+DPTAP. f^+ and f^- define reactive sites towards nucleophiles and electrophiles, respectively. The structures containing MEPs were rotated to facilitate visualization.

All the calculations presented so far were conducted in a solvent (via PCM). However, since the counterpoise method (for BSSE correction) is generally applied in vacuo, we also estimated the adsorption energies in the gas phase to evaluate the plausibility of the results. The relative values are compatible, with an average 3-fold overestimation for the gas-phase results. In particular, the adsorption energy for acephate +DPPC is 2.7–2.9 times the value for acephate+DPTAP and acephate +DODAB. This energy is compatible with a chemisorption process, however, it is associated with the hydrogen bond NH—O (phosphate) between acephate and DPPC. For DODAB and DPTAP the involved energies are compatible with a physisorption process. It is worth noting that the models with one acephate molecule close to the lipids (DODAB, DPTAP or DPPC) are not realistic for mono or bilayer systems. However, they are useful to estimate molecular features associated with local compounds reactivities and binding energies between acephate and the lipids, being thus complementary to the experiments. Moreover, as already mentioned, the lipid/lipid interactions can be estimated from electrostatic potentials.

In summary, from π-A isotherms, PM-IRRAS spectra, and theoretical calculations, one may propose the following interpretation: acephate has a strong (localized) negative character that explains both the attraction to the lipid cationic headgroups (choline and quaternary ammonium) and less evident interaction with the anionic phosphate groups. In the attractive interaction, O (negatively charged sites) and S (nucleophilic site) atoms of acephate could approach N of the lipid cationic headgroups, while for the lipid phosphate group the approach could be established through H atoms of acephate. This attraction could shift the π-A isotherm of the anionic lipids (DHP and DPPA) to smaller areas, which is not observed, probably as a consequence of the distribution of the positive portion of charge along the whole acephate molecule. The latter might favour the acephate molecules to be placed underneath DHP and DPPA monolayers.

As for the ordering of the alkyl chains inferred from the relative intensity between $\upsilon_s CH_2$ and $\upsilon_{as} CH_2$ bands, there is no indication of changes for DODAB, while there was an ordering effect for DPTAP and disordering one for DPPC. This pattern of behaviour may be related to the level of lipid tail organization in the neat monolayers. For instance, on an ultrapure water subphase, $RI_{DPPC} = 0.46$, $RI_{DODAB} = 0.55$, and $RI_{DPTAP} = 0.64$, indicating the alkyl chains are relatively more ordered for DPPC, followed by DODAB, then DPTAP. In the presence of acephate, RI for DODAB and DPTAP reaches similar values, 0.52 and 0.48 respectively, thus with similar chain ordering. This result might explain why DODAB RI does not change significantly in the presence of acephate, once its tails are already relatively ordered in water, which is not the

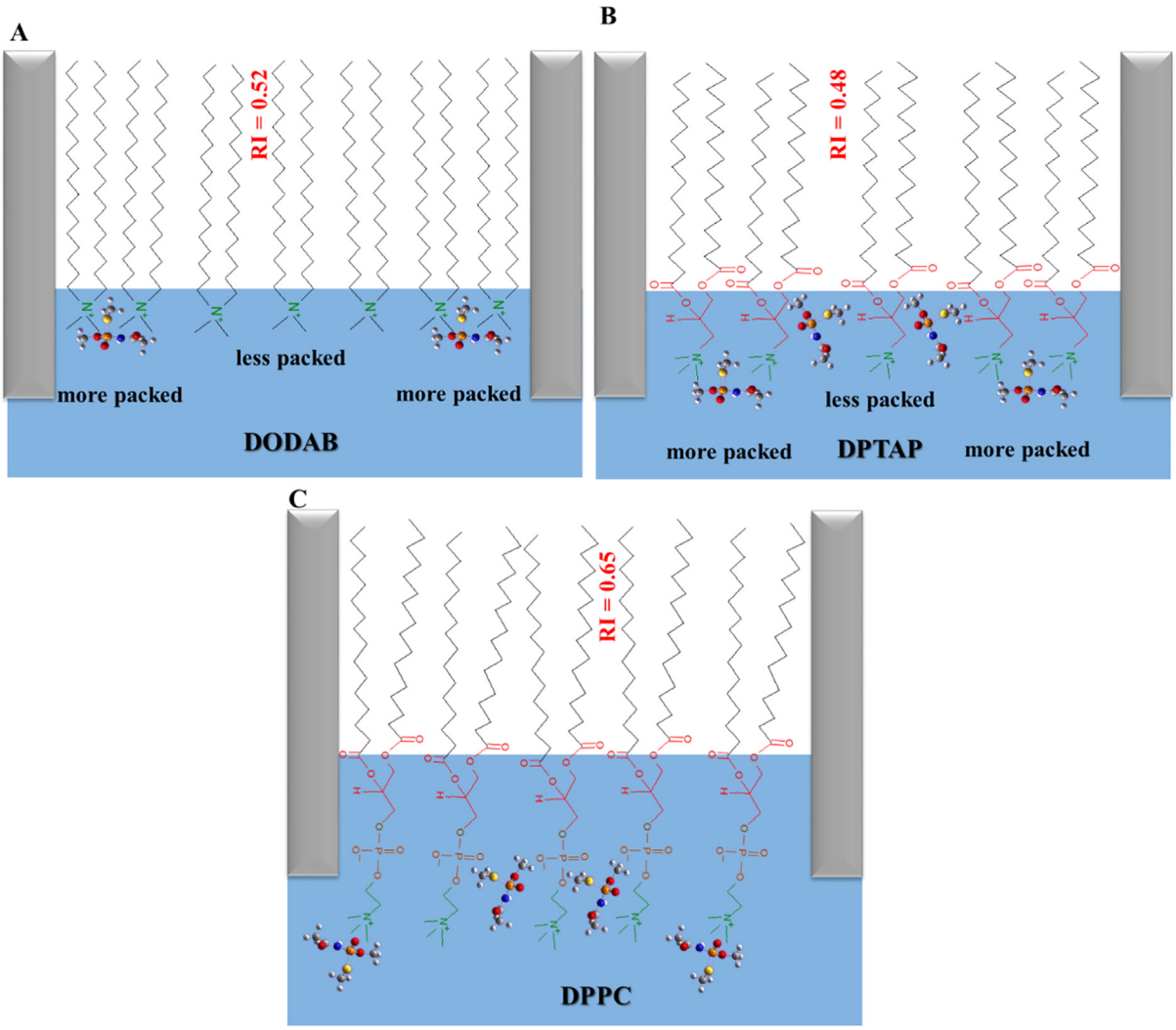

Fig. 8. Cartoons illustrating possible interactions between acephate and **(A)** DODAB; **(B)** DPTAP; and **(C)** DPPC monolayers on the Langmuir trough. The headgroups in lipid molecules are represented by the following colors - red: glycerol group; orange: phosphate group; green: choline group. Atoms of acephate molecules are represented by the colored spheres – yellow: sulfur; orange: phosphorus; red: oxygen; blue: nitrogen; gray: carbon; and white: hydrogen.

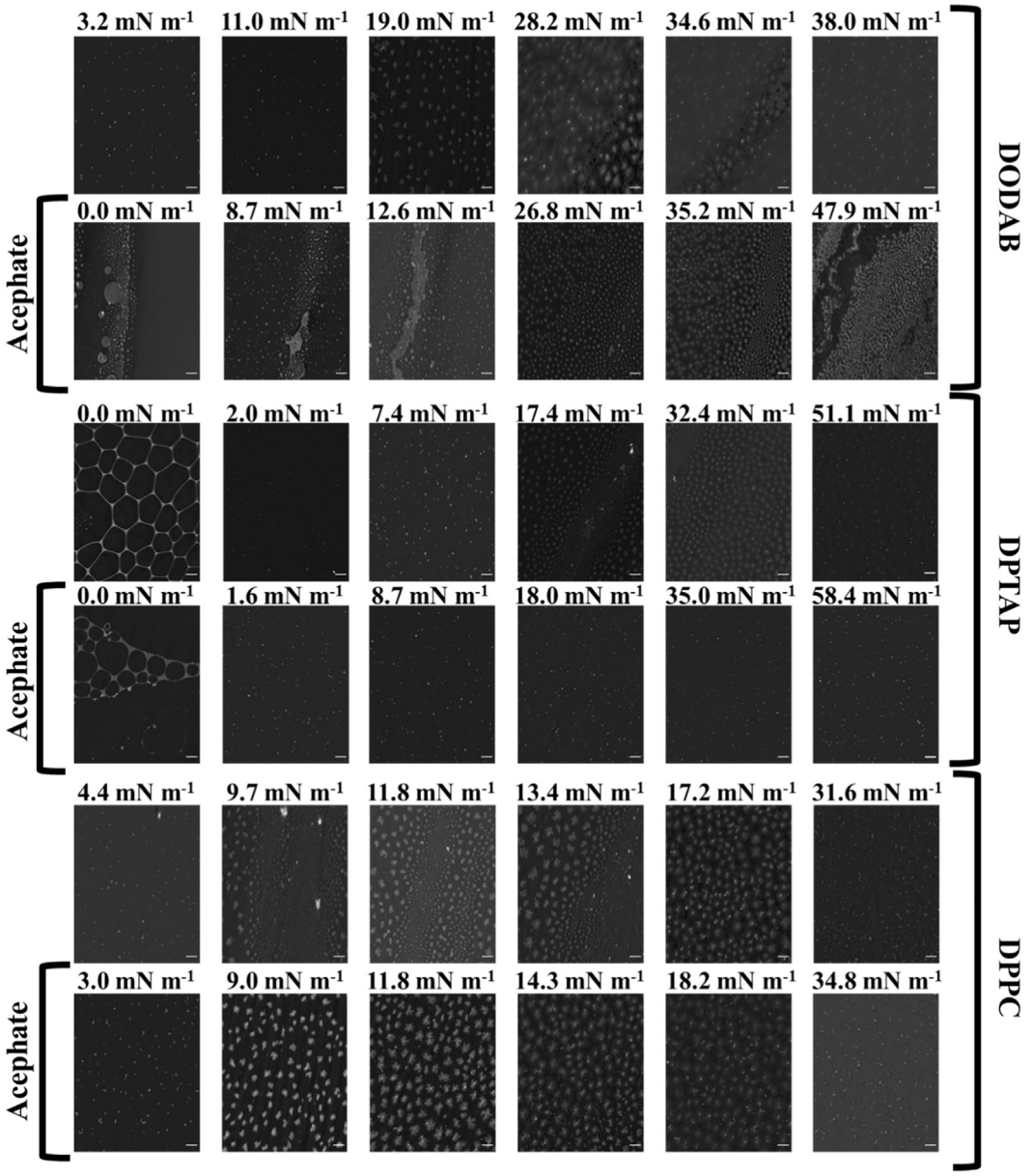

Fig. 9. BAM images of DODAB, DPTAP and DPPC monolayers in the absence and presence of acephate (10^{-4} M) at low and high surface pressures. Scale bar: 40 μm.

case of DPTAP. For DPPC, which is well-ordered on ultrapure water (in relation to DODAB and DPTAP), the attractive interaction of acephate with choline and phosphate groups leads to some loss in ordering. In a sequence of cartoons in Fig. 8 we illustrate the possible interactions of acephate with DODAB, DPTAP and DPPC, besides representing the lipid alkyl chain ordering/packing, on the basis of the qualitative interpretation just presented.

3.3. Morphological aspects of lipid monolayers in the presence of acephate

Fig. 9 shows BAM images of DODAB, DPTAP and DPPC Langmuir monolayers at different surface pressures at 25 °C. Small, circular lipid domains are seen in the expanded region of DODAB monolayer on ultrapure water (at 3 $mN.m^{-1}$), which are turned into flower-like domains (from ~10 to ~27 μm in diameter) upon compression, then becoming progressively more homogeneous at high pressures [59]. With acephate in the subphase, the formation of these very small structures starts at earlier stages of compression. For neat DPTAP monolayer, 'bubble-like' features appear at maximum expansion, which disappeared along the compression being replaced by small domains (at ~8 $mN.m^{-1}$), reaching a homogeneous state before monolayer collapse [60]. Incorporation of acephate led to more scarce and spaced domains, i.e. less densely packed. The shape and size of lipid domains in monolayers have been attributed to the attractive and repulsive forces during compression [61,62]. Thereby, the stabilization of positive charge in DODAB and DPTAP polar heads caused by acephate (displacing the π-A isotherms to smaller areas) increases monolayers rigidity, leading to a phase change in DODAB (from LE to LC). For DPTAP a similar change as that for DODAB was observed. This also caused a decrease in the size of the lipid micro domains, interfering in film homogeneity at high surface pressures. The BAM images for neat DPPC monolayer show typical domains of LE-LC phase being formed at 9.7 $mN.m^{-1}$ [63,64], which become more homogeneous during compression until disappearing at 31.6 $mN.m^{-1}$ (packed monolayer – LC phase). No significant changes are noted in the presence of acephate, which would indicate that acephate does not affect the monolayer morphology, consistent with the π-A isotherms and compressional modulus results for DPPC (Fig. 2).

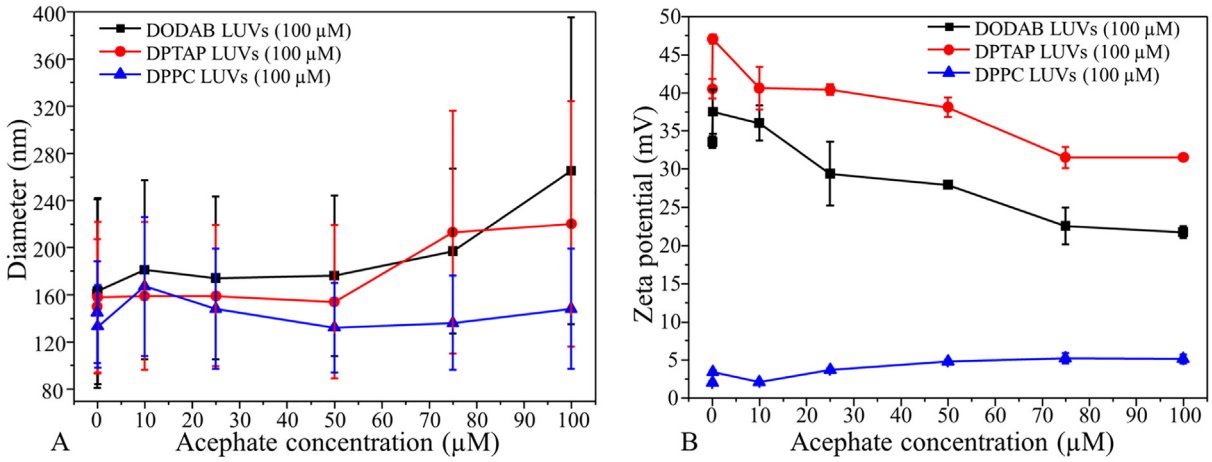

Fig. 10. (A) Diameters and (B) zeta potential of DODAB (black line with square points), DPTAP (red line with circle points) and DPPC (blue lines with triangle points) at different concentrations of acephate.

3.4. Effects of acephate on lipid vesicles

LUVs and GUVs of DODAB, DPTAP and DPPC were employed as bilayer models for cell membranes to compare the effects from acephate with those on Langmuir monolayers. The full data from DLS measurements with LUVs are given in the Supplementary Material (Table S1 and Fig. S5). The DLS distribution graphs had one peak for all LUVs in the absence of acephate, with diameters ranging from 140 to 170 nm, as expected since the final extrusion was performed using polycarbonate membranes with 0.1 μm pores. The PdI (Polydispersity Index) values also indicated monodisperse samples with uniform size distributions [65]. The diameter and zeta potential of LUVs of DODAB, DPTAP and DPPC are shown in Fig. 10. The positive zeta potentials for DODAB (33.5 ± 0.8 mV) and DPTAP (41 ± 1 mV) are expected from their positively charged head groups [66], while the near zero value (2.0 ± 0.2 mV) for DPPC is typical due its zwitterionic nature [67]. The diameter of DODAB and DPTAP LUVs increased with acephate concentration while the zeta potential became less positive. In contrast, no significant changes were observed for DPPC LUVs. The decrease in positive superficial charge for the cationic lipids are more prominent for the acephate concentrations of 75 and 100 μM, suggesting that acephate at concentrations close or equal to that of the vesicles (i.e. 100 μM) adsorb on cationic LUVs [68]. Since the PdI values indicate monodisperse vesicles without aggregation, the changes in zeta potential can be attributed to interactions between acephate and the lipid bilayers. This adsorption also increased the diameter of the cationic LUVs mainly at higher acephate concentrations.

Fig. 11 shows the GUVs phase contrast microscopy images in the absence (row A) and presence (row B) of acephate (0.8×10^{-4} M) acquired at 0 and 30 min of the experiment. All the vesicles in glucose solution have the spherical shape typical of these structures [69–71]. The vesicles of DODAB, DPTAP and DPPC should have a gel phase shape [25,70,72,73], since measurements were acquired below their phase transition temperature (room temperature ~ 23 °C; the phase transition temperature is 45 °C for DODAB [74], 42 °C for DPTAP [75] and 41 °C for DPPC [76]). Though ion-dipole interactions between acephate and the lipids were inferred in the experiments with Langmuir monolayers, no morphological changes or loss of phase contrast of GUVs take place during the period of observation (around 30 min). Although the zeta potentials for LUVs pointed to adsorption of acephate at the vesicles, this adsorption was not sufficient to induce microscopic changes in morphology or permeability of GUVs. The lack of changes at the giant vesicles can be related to the difference in their size, curvature and lipid packing, compared to the LUVs [77,78]. In subsidiary experiments we increased the acephate concentration by 10 fold (0.8×10^{-3} M), which is close to its limit of solubility, and still there was no significant effect on the GUVs.

Owing to the importance of a fluid phase to mimic more realistically the plasma membrane properties of eukaryotic cells [79], we also produced GUVs from the unsaturated lipid POPC which contains a carbon-carbon double bond in the alkyl chain and is at a fluid phase at room temperature [80]. The π-A isotherms in Fig. S1—C and the compressional modulus data in Fig. S2—F for POPC are consistent with the

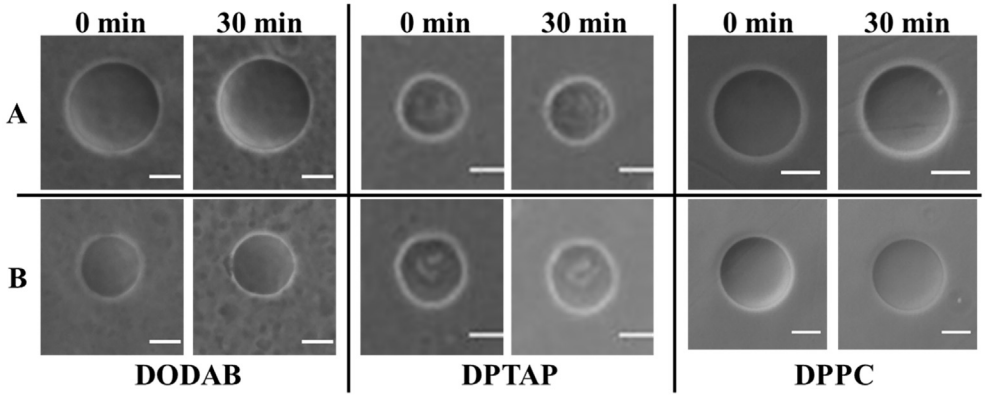

Fig. 11. DODAB, DPTAP, and DPPC GUVs in the absence (line A) and presence (line B) of acephate (0.8×10^{-4} M). Scale bar – 10 μm.

literature [81,82], and were not affected by incorporating acephate in the subphase, similarly to DPPC. Hence, regardless of the lipid phase, the isotherms of zwitterionic lipids are not affected by acephate. As observed with GUVs made of DPPC, those obtained from POPC in Fig. S6 did not have their morphology altered by acephate. We also performed additional experiments with DODAB and DPTAP GUVs, which were not affected by acephate either.

A straightforward comparison of the results from Langmuir monolayers and lipid bilayers is not possible because of some differences in the experimental procedures. Interaction of acephate may have been facilitated in Langmuir monolayers since it could adsorb from the subphase onto the monolayer while being formed – before being closely packed. The LUVs and GUVs, on the other hand, were already formed when acephate was added. One could nevertheless hypothesize that the complete absence of effects from acephate on the GUVs, even for the lipids whose monolayers were strongly affected, is evidence that acephate seems unable to induce disruption in the membrane. However, acephate at high concentrations (acephate/lipid ratios 1:1.3 and 1:1) did affect DODAB and DPTAP LUVs, which indicates that it can disrupt the membrane. The physiological action of acephate is then related to the binding on positively charged groups which could trigger other changes in the cell structure.

4. Conclusion

The pesticide acephate was found to possess a preferential interaction with Langmuir monolayers whose headgroups are positively charged. Indeed, acephate affected significantly the cationic DODAB and DPTAP monolayers, with their π-A isotherms being typical of more closely packed structures in the presence of acephate. From PM-IRRAS data, we observed that acephate is attracted by the quaternary ammonium (DODAB) and choline group (DPTAP), and its presence reduces the electrostatic repulsion between the lipid molecules. In contrast, acephate had negligible effects on the π-A isotherms of the zwitterionic DPPC and anionic DHP and DPPA, in spite of its interaction with phosphate groups and with the choline group of DPPC. These results are consistent with the localized negative character of acephate (against a non-localized portion of positive charges) as inferred from theoretical estimates. They also support the hypothesis according to which the physiological action of acephate is associated with binding to positively charged groups in the membrane. This conclusion was confirmed with the changes induced by acephate on DODAB and DPTAP LUVs, which were attributed to such binding. We hope that the findings presented here may help experimentalists and theoreticians to establish the conditions under which acephate is effective as insecticide without posing risks to human health.

CRediT authorship contribution statement

Luis F.C. Morato: Conceptualization, Methodology, Validation, Formal analysis, Investigation, Data curation, Writing - original draft, Visualization, Funding acquisition. **Gilia C.M. Ruiz:** Investigation, Formal analysis, Data curation, Writing - original draft. **Wallance M. Pazin:** Investigation, Formal analysis, Data curation, Writing - original draft. **Orisson P. Gomes:** Investigation, Formal analysis, Data curation. **Osvaldo N. Oliveira:** Resources, Visualization, Writing - original draft. **Augusto Batagin-Neto:** Formal analysis, Data curation, Writing - original draft. **Carlos J.L. Constantino:** Resources, Visualization, Supervision, Funding acquisition.

Declaration of Competing Interest

The authors declare that they have no known competing financial interests or personal relationships that could have appeared to influence the work reported in this paper.

Acknowledgements

FAPESP (2018/22214–6), CNPq, CAPES, and INCT/INEO.

Appendix A. Supplementary data

Supplementary data to this article can be found online at https://doi.org/10.1016/j.molliq.2021.115868.

References

[1] J.H. Carver, J. Bootman, M.C. Cimino, H.J. Esber, P. Kirby, B. Kirkhart, Z.A. Wong, J.A. MacGregor, Genotoxic potential of acephate technical: in vitro and in vivo effects, Toxicology. 35 (1985) 125–142, https://doi.org/10.1016/0300-483X(85)90027-7.
[2] ANVISA, Índice monográfico: A02 - Acefato, http://portal.anvisa.gov.br/documents/111215/117782/A02+-+Acefato/651fe170-9e1f-409f-93a3-b31b99e426b2 2017 (accessed October 2, 2017).
[3] Ascom/ANVISA, Publicada reclassificação toxicológica de agrotóxicos, 2019 http://portal.anvisa.gov.br/noticias/-/asset_publisher/FXrpx9qY7FbU/content/publicada-reclassificacao-toxicologica-de-agrotoxicos-/219201/pop_up?_101_INSTANCE_FXrpx9qY7FbU_viewMode=print&_101_INSTANCE_FXrpx9qY7FbU_languageId=en_US (accessed October 1, 2019).
[4] L. Zheng, F. Pi, Y. Wang, H. Xu, Y. Zhang, X. Sun, Photocatalytic degradation of Acephate, Omethoate, and methyl parathion by Fe3O4@SiO2@mTiO2 nanomicrospheres, J. Hazard. Mater. 315 (2016) 11–22, https://doi.org/10.1016/j.jhazmat.2016.04.064.
[5] ANVISA, Programa de Análise de Resíduos de Agrotóxicos em Alimentos (PARA): relatório das amostras analisadas no período de 2017–2018, Agência Nac, Vigilância Sanitária 136 (2019) https://doi.org/10.1017/CBO9781107415324.004.
[6] W.A. Pignati, F.A.N. de S E Lima, S.S. de Lara, M.L.M. Correa, J.R. Barbosa, L.H.D.C. Leão, M.G. Pignatti, Distribuição espacial do uso de agrotóxicos no Brasil: uma ferramenta para a Vigilância em Saúde, Cien. Saude Colet. 22 (2017) 3281–3293, https://doi.org/10.1590/1413-812320172210.17742017.
[7] G.B. Jena, S.P. Bhunya, Mutagenicity of an organophosphate insecticide acephate: an in vivo study in chicks, Mutagenesis. 9 (1994) 319–324.
[8] M. Mandi, S. Khatun, P. Rajak, A. Mazumdar, S. Roy, Potential risk of organophosphate exposure in male reproductive system of a non-target insect model Drosophila melanogaster, Environ. Toxicol. Pharmacol. 74 (2020) 103308, https://doi.org/10.1016/j.etap.2019.103308.
[9] C.F. Sampaio, K.V. Prates, G.E.M.L. Siervo, P.C. de F Mathias, G.S.A. Fernandes, Impairment of testicular development in rats exposed to acephate during maternal gestation and lactation, Environ. Sci. Pollut. Res. 27 (2020) 5482–5488, https://doi.org/10.1007/s11356-019-07209-0.
[10] T. Takayasu, H. Yamamoto, Y. Ishida, M. Nosaka, Y. Kuninaka, E. Shimada, M. Kawaguchi, A. Kimura, T. Kondo, Postmortem distribution of acephate and its metabolite methamidophos in body fluids and organ tissues of an intoxication case, Forensic Sci. Int. 300 (2019) e38–e43, https://doi.org/10.1016/j.forsciint.2019.02.015.
[11] K. Gholivand, A.A. Ebrahimi Valmoozi, H.R. Mahzouni, S. Ghadimi, R. Rahimi, Molecular docking and QSAR studies: noncovalent interaction between acephate analogous and the receptor site of human Acetylcholinesterase, J. Agric. Food Chem. 61 (2013) 6776–6785, https://doi.org/10.1021/jf401092h.
[12] S. Ghadimi, S.L. Mousavi, Z. Rahnama, M. Rahimi, Synthesis and Characterization of O,S-Dimethylphosphoramidothioate and N-Acetyl O,S-Dimethylphosphoramidothioate, Phosphorus Sulfur Silicon Relat. Elem. 185 (2010) 347–354, https://doi.org/10.1080/10426500902797079.
[13] R. Palkhade, S. Yadav, S. Mishra, J. Muhamed, Acute oral toxicity of pesticide combination (acephate 50% and imidacloprid 1.8% as active ingredients) in Sprague-Dawley rats, Vet. World. 11 (2018) 1291–1297, https://doi.org/10.14202/vetworld.2018.1291-1297.
[14] S.B. Gould, Membranes and evolution, Curr. Biol. 28 (2018) R381–R385, https://doi.org/10.1016/j.cub.2018.01.086.
[15] J. Knobloch, D.K. Suhendro, J.L. Zieleniecki, J.G. Shapter, I. Köper, Membrane–drug interactions studied using model membrane systems, Saudi J. Biol. Sci. 22 (2015) 714–718, https://doi.org/10.1016/j.sjbs.2015.03.007.
[16] I. Langmuir, The constitution and fundamental properties of solids and liquids. Part I. solids, J. Am. Chem. Soc. 38 (1916) 2221–2295, https://doi.org/10.1021/ja02268a002.
[17] I. Langmuir, The constitution and fundamental properties of solids and liquids. II. Liquids. 1, J. Am. Chem. Soc. 39 (1917) 1848–1906, https://doi.org/10.1021/ja02254a006.
[18] K.K. Das, J.D. Unsay, A.J. Garcia-Saez, Microscopy of model membranes: understanding how Bcl-2 proteins mediate apoptosis, FEMS Microbiol. Lett. (2015) 63–97, https://doi.org/10.1016/bs.adplan.2015.01.002.
[19] M. Patterson, H.J. Vogel, E.J. Prenner, Biophysical characterization of monofilm model systems composed of selected tear film phospholipids, Biochim. Biophys. Acta Biomembr. 1858 (2016) 403–414, https://doi.org/10.1016/j.bbamem.2015.11.025.
[20] P. Nigam, Equilibrium penetration of pluronic F-68 in lipid monolayers, Chem. Phys. Lipids 228 (2020) 104888, https://doi.org/10.1016/j.chemphyslip.2020.104888.
[21] A. Martín-Molina, T. Del Castillo-Santaella, Y. Yang, J. Maldonado-Valderrama, Condensation of model lipid films by cholesterol: specific ion effects, Coatings. 9 (2019) 474, https://doi.org/10.3390/coatings9080474.
[22] C.M.N. Mendonca, D.T. Balogh, S.C. Barbosa, T.E. Sintra, S.P.M. Ventura, L.F.G. Martins, P. Morgado, E.J.M. Filipe, J.A.P. Coutinho, O.N. Oliveira, A. Barros-Timmons, Understanding the interactions of imidazolium-based ionic liquids with cell membrane

models, Phys. Chem. Chem. Phys. 20 (2018) 29764–29777, https://doi.org/10.1039/c8cp05035j.
[23] A. Sakai, A.P. de Sousa Mesquista, H.B. Nader, C.C. Lopes, W. Nakanishi, K. Ariga, L. Caseli, The lipid composition affects Trastuzumab adsorption at monolayers at the air-water interface, Chem. Phys. Lipids 227 (2020) 104875, https://doi.org/10.1016/j.chemphyslip.2020.104875.
[24] C. Pereira-Leite, D. Lopes-de-Campos, P. Fontaine, I.M. Cuccovia, C. Nunes, S. Reis, Licofelone-DPPC interactions: Putting membrane lipids on the radar of drug development, Molecules 24 (2019)https://doi.org/10.3390/molecules24030516.
[25] L.S. Martins, D.A. Nomura, E.L. Duarte, K.A. Riske, M.T. Lamy, J.H.K. Rozenfeld, Structural characterization of cationic DODAB bilayers containing C24:1 β-glucosylceramide, Biochim. Biophys. Acta Biomembr. 1861 (2019) 643–650, https://doi.org/10.1016/j.bbamem.2018.12.018.
[26] M.I. Angelova, D.S. Dimitrov, Liposome electroformation, Faraday Discuss. Chem. Soc. 81 (1986) 303, https://doi.org/10.1039/dc9868100303.
[27] M.I. Angelova, S. Soléau, P. Méléard, F. Faucon, P. Bothorel, Preparation of giant vesicles by external AC electric fields. Kinetics and applications, Trends Colloid Interface Sci. VI, Steinkopff, Darmstadt 1992, pp. 127–131, https://doi.org/10.1007/BFb0116295.
[28] J. Nam, T.K. Vanderlick, P.A. Beales, Formation and dissolution of phospholipid domains with varying textures in hybrid lipo-polymersomes, Soft Matter 8 (2012) 7982, https://doi.org/10.1039/c2sm25646k.
[29] A. Weinberger, F.C. Tsai, G.H. Koenderink, T.F. Schmidt, R. Itri, W. Meier, T. Schmatko, A. Schröder, C. Marques, Gel-assisted formation of giant unilamellar vesicles, Biophys. J. 105 (2013) 154–164, https://doi.org/10.1016/j.bpj.2013.05.024.
[30] P.J. Stephens, F.J. Devlin, C.F. Chabalowski, M.J. Frisch, Ab initio calculation of vibrational absorption and circular Dichroism spectra using density functional force fields, J. Phys. Chem. 98 (1994) 11623–11627, https://doi.org/10.1021/j100096a001.
[31] S.H. Vosko, L. Wilk, M. Nusair, Accurate spin-dependent electron liquid correlation energies for local spin density calculations: a critical analysis, Can. J. Phys. 58 (1980) 1200–1211, https://doi.org/10.1139/p80-159.
[32] C. Lee, W. Yang, R.G. Parr, Development of the Colle-Salvetti correlation-energy formula into a functional of the electron density, Phys. Rev. B 37 (1988) 785–789, https://doi.org/10.1103/PhysRevB.37.785.
[33] A.D. Becke, Density-functional thermochemistry. III. The role of exact exchange, J. Chem. Phys. 98 (1993) 5648–5652, https://doi.org/10.1063/1.464913.
[34] T. Yanai, D.P. Tew, N.C. Handy, A new hybrid exchange–correlation functional using the coulomb-attenuating method (CAM-B3LYP), Chem. Phys. Lett. 393 (2004) 51–57, https://doi.org/10.1016/j.cplett.2004.06.011.
[35] J. Tomasi, B. Mennucci, R. Cammi, Quantum mechanical continuum solvation models, Chem. Rev. 105 (2005) 2999–3094, https://doi.org/10.1021/cr9904009.
[36] M.J. Frisch, G.W. Trucks, H.B. Schlegel, G.E. Scuseria, M.A. Robb, J.R. Cheeseman, G. Scalmani, V. Barone, G.A. Petersson, X. Nakatsuji, H. Li, M. Caricato, A.V. Marenich, J. Bloino, B.G. Janesko, R. Gomperts, B. Mennucci, H.P. Hratchian, J.V. Ortiz, A.F. Izmaylov, J.L. Sonnenberg, D. Williams-Young, F. Ding, F. Lipparini, F. Egidi, J. Goings, B. Peng, A. Petrone, T. Henderson, D. Ranasinghe, V.G. Zakrzewski, N. Gao, J. Rega, G. Zheng, W. Liang, M. Hada, M. Ehara, K. Toyota, R. Fukuda, J. Hasegawa, M. Ishida, T. Nakajima, Y. Honda, O. Kitao, H. Nakai, T. Vreven, K. Throssell, J. Montgomery, J. A, J.E. Peralta, F. Ogliaro, M.J. Bearpark, J.J. Heyd, E.N. Brothers, K.N. Kudin, V.N. Staroverov, T.A. Keith, R. Kobayashi, J. Normand, K. Raghavachari, A.P. Rendell, J.C. Burant, S.S. Iyengar, J. Tomasi, M. Cossi, J.M. Millam, M. Klene, C. Adamo, R. Cammi, J.W. Ochterski, R.L. Martin, K. Morokuma, O. Farkas, J.B. Foresman, D.J. Fox, Gaussian 16, Revision C.01, 2016 http://gaussian.com/ (accessed September 1, 2020).
[37] F. Neese, The ORCA program system, WIREs Comput. Mol. Sci. 2 (2012) 73–78, https://doi.org/10.1002/wcms.81.
[38] P. Geerlings, F. De Proft, W. Langenaeker, Conceptual density functional theory, Chem. Rev. 103 (2003) 1793–1874, https://doi.org/10.1021/cr990029p.
[39] W. Yang, W.J. Mortier, The use of global and local molecular parameters for the analysis of the gas-phase basicity of amines, J. Am. Chem. Soc. 108 (1986) 5708–5711, https://doi.org/10.1021/ja00279a008.
[40] E.G. Lewars, Computational Chemistry, 2nd ed. Springer Netherlands, Dordrecht, 2011https://doi.org/10.1007/978-90-481-3862-3.
[41] R.A. Maia, G. Ventorim, A. Batagin-Neto, Reactivity of lignin subunits: the influence of dehydrogenation and formation of dimeric structures, J. Mol. Model. 25 (2019) 228, https://doi.org/10.1007/s00894-019-4130-4.
[42] G.G.B. Alves, F.C. Lavarda, C.F.O. Graeff, A. Batagin-Neto, Reactivity of eumelanin building blocks: a DFT study of monomers and dimers, J. Mol. Graph. Model. 98 (2020) 107609, https://doi.org/10.1016/j.jmgm.2020.107609.
[43] F. De Proft, C. Van Alsenoy, A. Peeters, W. Langenaeker, P. Geerlings, Atomic charges, dipole moments, and Fukui functions using the Hirshfeld partitioning of the electron density, J. Comput. Chem. 23 (2002) 1198–1209, https://doi.org/10.1002/jcc.10067.
[44] R.K. Roy, S. Pal, K. Hirao, On non-negativity of Fukui function indices, J. Chem. Phys. 110 (1999) 8236–8245, https://doi.org/10.1063/1.478792.
[45] L.E. Chirlian, M.M. Francl, Atomic charges derived from electrostatic potentials: a detailed study, J. Comput. Chem. 8 (1987) 894–905, https://doi.org/10.1002/jcc.540080616.
[46] S.F. Boys, F. Bernardi, The calculation of small molecular interactions by the differences of separate total energies. Some procedures with reduced errors, Mol. Phys. 19 (1970) 553–566, https://doi.org/10.1080/00268977000101561.
[47] A.K. de Brito, C.S.F. Nordi, L. Caseli, Algal polysaccharides as matrices for the immobilization of urease in lipid ultrathin films studied with tensiometry and vibrational spectroscopy: physical–chemical properties and implications in the enzyme activity, Colloids Surf. B: Biointerfaces 135 (2015) 639–645, https://doi.org/10.1016/j.colsurfb.2015.08.033.
[48] A. Tsanova, A. Jordanova, T. Dzimbova, T. Pajpanova, E. Golovinsky, Z. Lalchev, Interaction of methionine–enkephalins with raft-forming lipids: monolayers and BAM experiments, Amino Acids 46 (2014) 1159–1168, https://doi.org/10.1007/s00726-013-1647-1.
[49] D. Marsh, Lateral pressure in membranes, Biochim. Biophys. Acta Rev. Biomembr. 1286 (1996) 183–223, https://doi.org/10.1016/S0304-4157(96)00009-3.
[50] W. Probst, D. Möbius, H. Rahmann, Modulatory effects of different temperatures and Ca2+ concentrations on gangliosides and phospholipids in monolayers at air/water interfaces and their possible functional role, Cell. Mol. Neurobiol. 4 (1984) 157–176, https://doi.org/10.1007/BF00711002.
[51] R.L. Cruz Gomes da Silva, H.F. Oliveira da Silva, L.H. da Silva Gasparotto, L. Caseli, How the interaction of PVP-stabilized Ag nanoparticles with models of cellular membranes at the air-water interface is modulated by the monolayer composition, J. Colloid Interface Sci. 512 (2018) 792–800, https://doi.org/10.1016/j.jcis.2017.10.091.
[52] L.N. Furini, L.F.C. Morato, D.S. Olivier, M. Lemos, E. Feitosa, C.J.L. Constantino, Interactions of lipid polar headgroups with Carbendazim fungicide, J. Nanosci. Nanotechnol. 19 (2019) 3734–3743, https://doi.org/10.1166/jnn.2019.16739.
[53] J.T. Davies, E.K. Rideal, Interfacial Phenomena, Interfacial Phenom, Elsevier 1961, p. 265, https://doi.org/10.1016/B978-0-12-395609-5.50015-4.
[54] K. Sugat, J.F. Rusling, Structural characterization of surfactant and clay-surfactant films of micrometer thickness by FT-IR spectroscopy, Langmuir. (1993) 3649–3655, https://doi.org/10.1021/la00036a048.
[55] F. Korkmaz, F. Severcan, Effect of progesterone on DPPC membrane: evidence for lateral phase separation and inverse action in lipid dynamics, Arch. Biochem. Biophys. 440 (2005) 141–147, https://doi.org/10.1016/j.abb.2005.06.013.
[56] R.F. Vázquez, M.A. Daza, F.J. Pavinatto, M.L. Fanani, Impact of sphingomyelin acyl chain (16 : 0 vs 24 : 1) on the interfacial properties of Langmuir monolayers : A PM-IRRAS study, Colloids Surf. B: Biointerfaces 173 (2019) 549–556, https://doi.org/10.1016/j.colsurfb.2018.10.018.
[57] G.M. Stunges, C.S. Martin, G.C.M. Ruiz, O.N. Oliveira, C.J.L. Constantino, P. Alessio, Interaction between 17 α-ethynylestradiol hormone with Langmuir monolayers: the role of charged headgroups, Colloids Surf. B: Biointerfaces 158 (2017) 627–633, https://doi.org/10.1016/j.colsurfb.2017.07.034.
[58] L.S.A. Pereira, S.A. Camacho, A.A. Malfatti-Gasperini, K. Jochelavicius, T.M. Nobre, O.N. Oliveira, P.H.B. Aoki, Evidence of photoinduced lipid hydroperoxidation in Langmuir monolayers containing eosin Y, Colloids Surf. B: Biointerfaces 171 (2018) 682–689, https://doi.org/10.1016/j.colsurfb.2018.08.002.
[59] A.M. Gonçalves da Silva, R.S. Romão, A. Lucero Caro, J.M. Rodriguez Patino, Memory effects on the interfacial characteristics of dioctadecyldimethylammonium bromide monolayers at the air–water interface, J. Colloid Interface Sci. 270 (2004) 417–425, https://doi.org/10.1016/j.jcis.2003.11.002.
[60] B. Gzyl-Malcher, M. Filek, G. Brezesinski, Influence of cadmium and Selenate on the interactions between hormones and phospholipids, Langmuir. 25 (2009) 13071–13076, https://doi.org/10.1021/la901653y.
[61] L. Zou, J. Wang, P. Basnet, E.K. Mann, Line tension and structure of smectic liquid-crystal multilayers at the air-water interface, Phys. Rev. E - Stat. Nonlinear, Soft Matter Phys. 76 (2007) 1–6, https://doi.org/10.1103/PhysRevE.76.031602.
[62] S. Rivière, S. Hénon, J. Meunier, G. Albrecht, M.M. Boissonnade, A. Baszkin, Electrostatic pressure and line tension in a Langmuir monolayer, Phys. Rev. Lett. 75 (1995) 2506–2509, https://doi.org/10.1103/PhysRevLett.75.2506.
[63] M.E. Mariani, M.E. Sánchez-Borzone, D.A. García, Effects of bioactive monoterpenic ketones on membrane organization. A langmuir film study, Chem. Phys. Lipids 198 (2016) 39–45, https://doi.org/10.1016/j.chemphyslip.2016.05.002.
[64] W.M. Pazin, G.C.M. Ruiz, O.N. de Oliveira, C.J.L. Constantino, Interaction of Artepillin C with model membranes: effects of pH and ionic strength, Biochim. Biophys. Acta Biomembr. 1861 (2019) 410–417, https://doi.org/10.1016/j.bbamem.2018.11.008.
[65] A.L. Rubio, M.J.F. Rovira, M.M. Sanz, L.G. Gómez-Mascaraque (Eds.), Nanomaterials For Food Applications, Academic Press, an imprint of Elsevier, Amsterdam, Netherlands, 2019.
[66] G.A.T. Kaminski, M.R. Sierakowski, R. Pontarolo, R.A. De Freitas, Comparison between the interactions of the cationic surfactant DODAB with xanthan and galactomannan, Carbohydr. Polym. 115 (2015) 478–484, https://doi.org/10.1016/j.carbpol.2014.08.111.
[67] M.A. Morini, M.B. Sierra, V.I. Pedroni, L.M. Alarcon, G.A. Appignanesi, E.A. Disalvo, Influence of temperature, anions and size distribution on the zeta potential of DMPC, DPPC and DMPE lipid vesicles, Colloids Surf. B: Biointerfaces 131 (2015) 54–58, https://doi.org/10.1016/j.colsurfb.2015.03.054.
[68] P. Maity, B. Saha, G. Suresh Kumar, S. Karmakar, Effect of Zwitterionic phospholipid on the interaction of cationic membranes with monovalent sodium salts, Langmuir. 34 (2018) 9810–9817, https://doi.org/10.1021/acs.langmuir.8b01792.
[69] V. Šuštar, J. Zelko, P. Lopalco, S. Lobasso, A. Ota, N.P. Ulrih, A. Corcelli, V. Kralj-Iglič, Morphology, biophysical properties and protein-mediated fusion of Archaeosomes, PLoS One 7 (2012), e39401, https://doi.org/10.1371/journal.pone.0039401.
[70] L.A. Bagatolli, E. Gratton, Two-photon fluorescence microscopy observation of shape changes at the phase transition in phospholipid giant unilamellar vesicles, Biophys. J. 77 (1999) 2090–2101, https://doi.org/10.1016/S0006-3495(99)77050-5.
[71] P. Peterlin, V. Arrigler, Electroformation in a flow chamber with solution exchange as a means of preparation of flaccid giant vesicles, Colloids Surf. B: Biointerfaces 64 (2008) 77–87, https://doi.org/10.1016/j.colsurfb.2008.01.004.
[72] A.E. McKiernan, T.V. Ratto, M.L. Longo, Domain growth, shapes, and topology in cationic lipid bilayers on Mica by fluorescence and atomic force microscopy, Biophys. J. 79 (2000) 2605–2615, https://doi.org/10.1016/S0006-3495(00)76499-X.
[73] D.L. Perrier, L. Rems, M.T. Kreutzer, P.E. Boukany, The role of gel-phase domains in electroporation of vesicles, Sci. Rep. 8 (2018) 4758, https://doi.org/10.1038/s41598-018-23097-9.

[74] R.O. Brito, E.F. Marques, Neat DODAB vesicles: effect of sonication time on the phase transition thermodynamic parameters and its relation with incomplete chain freezing, Chem. Phys. Lipids 137 (2005) 18–28, https://doi.org/10.1016/j.chemphyslip.2005.05.001.
[75] G.D. Bothun, A. Lelis, Y. Chen, K. Scully, L.E. Anderson, M.A. Stoner, Multicomponent folate-targeted magnetoliposomes: design, characterization, and cellular uptake, Nanomed. Nanotechnol. Biol. Med. 7 (2011) 797–805, https://doi.org/10.1016/j.nano.2011.02.007.
[76] X. Xu, A. Costa, D.J. Burgess, Protein encapsulation in Unilamellar liposomes: high encapsulation efficiency and a novel technique to assess lipid-protein interaction, Pharm. Res. 29 (2012) 1919–1931, https://doi.org/10.1007/s11095-012-0720-x.
[77] M.E. Herbig, K.M. Weller, H.P. Merkle, Reviewing biophysical and cell biological methodologies in cell-penetrating peptide (CPP) research, Crit. Rev. Ther. Drug Carr. Syst. 24 (2007) 203–255, https://doi.org/10.1615/CritRevTherDrugCarrierSyst.v24.i3.10.
[78] M.S. Terakawa, Y. Lin, M. Kinoshita, S. Kanemura, D. Itoh, T. Sugiki, M. Okumura, A. Ramamoorthy, Y.-H. Lee, Impact of membrane curvature on amyloid aggregation, Biochim. Biophys. Acta Biomembr. 1860 (2018) 1741–1764, https://doi.org/10.1016/j.bbamem.2018.04.012.
[79] H.J. Kaiser, M.A. Surma, F. Mayer, I. Levental, M. Grzybek, R.W. Klemm, S. Da Cruz, C. Meisinger, V. Müller, K. Simons, D. Lingwood, Molecular convergence of bacterial and eukaryotic surface order, J. Biol. Chem. 286 (2011) 40631–40637, https://doi.org/10.1074/jbc.M111.276444.
[80] K.L. Koster, M.S. Webb, G. Bryant, D.V. Lynch, Interactions between soluble sugars and POPC (1-palmitoyl-2-oleoylphosphatidylcholine) during dehydration: vitrification of sugars alters the phase behavior of the phospholipid, Biochim. Biophys. Acta Biomembr. 1193 (1994) 143–150, https://doi.org/10.1016/0005-2736(94)90343-3.
[81] K. Węder, M. Mach, K. Hąc-Wydro, P. Wydro, Studies on the interactions of anticancer drug - Minerval - with membrane lipids in binary and ternary Langmuir monolayers, Biochim. Biophys. Acta Biomembr. 1860 (2018) 2329–2336, https://doi.org/10.1016/j.bbamem.2018.05.019.
[82] E.J. Grasso, R.G. Oliveira, B. Maggio, Surface interactions, thermodynamics and topography of binary monolayers of insulin with dipalmitoylphosphatidylcholine and 1-palmitoyl-2-oleoylphosphatidylcholine at the air/water interface, J. Colloid Interface Sci. 464 (2016) 264–276, https://doi.org/10.1016/j.jcis.2015.11.034.